Journal of New Technology and Materials (JNTM)
J. New Technol. Mater.
Vol. 12, N°02 (2022)80-88

OEB Univ. Publish. Co.

Computational studies on side chain effects of five membered ring sulphur heterocycles on the corrosion inhibition of iron metal

Thomas Aondofa Nyijime[a], Abdullahi Muhammad Ayuba[b]* and Habibat Faith Chahul[a]

[a]*Department of Chemistry, College of Sciences, Federal University of Agriculture, Makurdi, 970212, Nigeria.*
[b]*Department of Pure and Industrial Chemistry, Faculty of Physical Sciences, Bayero University, Kano, 700023, Nigeria.*
* Correspondence author email: ayubaabdullahi@buk.edu.ng

Received date: Sep. 21, 2022 ; accepted date: Nov. 5, 2022

Abstract

When exposed to harsh settings, iron, one of the most useful metals on earth, is known to corrode. To explore the ability to suppress corrosion, a variety of techniques have been employed, including computational methods. Quantum chemical and molecular dynamic modeling techniques were used to study the corrosion inhibitory effects of thiophene (THIO) and its derivatives, including 2-thiophene carboxylic acid (2-TCA) and 2-thiophene carboxylic acid hydrazide (2-TCAH), on the surface of iron metal. Results from quantum chemistry investigations of the molecules' local and global reactivity demonstrate their potential as inhibitors of iron surface corrosion, with THIO appearing to have the most promise. Quenched molecular dynamic simulations of the examined molecules' adsorption and binding energies on the iron surface revealed that the interaction is quite weak, with values found below the ±100kcal/mol threshold value. As a result, the molecules obey the physical adsorption mechanism in the following order: THIO > 2-TCA > 2-TCAH. This indicates that the molecules are weakly adsorbed onto the surface of Fe(1 1 0) through van der Waals forces. The THIO molecule has a higher degree of planarity than the other derivatives since it doesn't have any side chains that could interfere with its ability to adsorb to the surface of the iron metal.

Keywords: Thiophene; corrosion inhibition; molecular dynamics; quantum chemical parameters; physical adsorption

1. Introduction

Due to the widespread use of acidic solutions by most industries, particularly in the areas of acid pickling of iron and steel, chemical cleaning and processing, ore production, and oil well acidification, which cannot be avoided in routine processes, corrosion of iron and steel has become a topic of interest. Therefore, these have a considerable negative impact on the environment around the metal, necessitating measures to lessen, stop, or delay the damaging process [1]. The usage of chemicals, which are often heterocyclic in nature, as either existing inhibitor molecules or plants extract as promising inhibitors to prevent or restrict the deterioration of materials have been used as a result of these significant effects generated by acidic solutions [2]. A significant amount of research has been done on the mechanism by which inorganic, organic, or polymeric chemicals limit the corrosion of iron and steel in acidic, basic, and salt media [3-6]. Due to the existence of heterocyclic compounds and other compounds containing π-electrons in their molecules, as well as polar groups containing n-electron atoms like sulfur, oxygen, and nitrogen, these chemicals have been proving to possess an inhibitory effect [7]. These substances have a propensity to adsorb on metal surfaces, block the active sites, and so reduce the rate of disintegration. It is important to keep in mind that the effectiveness of the inhibitor molecule depends not only on the immediate environment it interacts with or comes into contact with, or the type of metal surface, but also on the inhibitor's structure, which includes its molecular size, charge density, mode of adsorption, number of adsorption active sites, and ability to form metallic complexes [8–12]. Experimental studies on thiophene derivatives as metal corrosion inhibitors have shown that they are both safe and effective for the environment [13].

Fouda et al. [13] used techniques such as weight loss, potentiodynamic polarization, electrochemical frequency modulation (EFM), and electrochemical impedance spectroscopy (EIS) to investigate the inhibitory effect of various thiophene derivatives in 1M HCl on the corrosion of carbon steel. Similar findings are obtained using all methods, and it is discovered that these substances are inhibitors of mixed types. In their studies, inhibition efficiency rose with increasing inhibitor concentration and decreased with increasing temperature.

It becomes extremely difficult and frequently expensive to describe the inhibitory mechanism in detail through an experimental approach. Therefore, it has become simpler to examine the molecular structure as one of the key factors influencing the adsorption of organic molecules on the metal surface with the introduction of computer software including quantum chemistry technique and molecular modeling methodologies. Theoretically, the chemicals' inhibitory effectiveness can be attributed to their molecular characteristics.

In this study, the thiophene (THIO) molecule was compared to two other thiophene derivatives; 2-thiophene carboxylic acid (2-TCA) and 2-thiophene carboxylic acid hydrazide (2-TCAH). These are organic substances with nearly the same chemical structure base, so the selection of these compounds was based on

molecular structure considerations. As a result, the differences in their inhibition properties should primarily be attributable to these compounds' different electronic structures. Both molecular dynamic simulation and quantum chemical parameters were researched and compared to experimental findings [13]. This research aims to confirm experimental results by identifying a feasible mechanism for the corrosion inhibition effectiveness of inhibitors on iron metal surfaces. Analysis was done on the relationships between other quantum chemical parameters, including E_{HOMO} and $E_{LUM}O$, charge density distribution, energy gap, dipole moment, Fukui functions, global and local reactivities, and the inhibition efficacy of the two tested thiophene derivatives in relation to the reference molecule thiophene. Figure 1 depicts the chemical structures of the molecules under study.

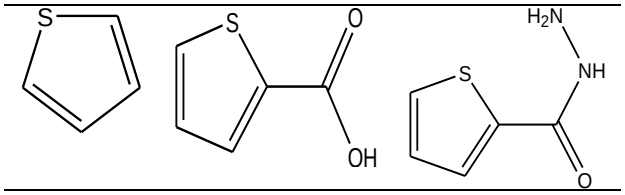

a) Thiophene (THIO)	b) 2-thiophene carboxylic acid (2-TCA)	c) 2-thiophene carboxylic acid hydrazide (2-TCAH)

Figure 1. Chemical structure of a) Thiophene, b) 2-thiophene carboxylic acid and b) 2-thiophene carboxylic acid hydrazide

2. Computational Methods

2.1. Quantum chemical parameters

Using the ChemDraw Ultra 7.0.3 CambridgeSoft program, molecular diagrams of 2-thiophene carboxylic acid, 2-thiophene carboxylic acid hydrazide, and thiophene, the reference molecule, were created. The complete set of drawn molecules was saved as an MDL Molfile (*.mol). The DMol^3 program included in BIOVIA Materials studio 8.0 (Accelrys, Inc.) was used to carry out a procedure known as geometry optimization on the molecules' torsional and conformational energies [14]. The relevant chemicals were imported from ChemDraw onto the surface of the newly formed 3D atomistic document in the material studio. The quantum chemistry calculations based on the ideas of Density Functional Theory (DFT) were performed using the DMol^3 program. B3LYP functional with "double-numeric plus polarization" (DNP) basis set in aqueous phase model was used to calculate quantum chemical parameters [2]. Frontier molecular orbital energies (E_{HOMO} and E_{LUMO}), total electron density, and Fukui indices were assessed in order to determine the active centres as well as local and global reactivities of the compounds with respect to their corrosion inhibition efficiency [15]. The electronegativity (χ), global hardness (η), and global softness (σ), as well as the global electrophilicity index (ω), nucleophilicity (ε), energy of back donation (ΔE_{b-d}), fraction of electron(s) transfer (ΔN), and the Fukui function f(r) were each evaluated and related to the ionization potential, IP, and electron affinity EA of each inhibitor molecule. These parameters will further provide insight into the chemical reactivity [16].

IE: Ionization energy (eV) $IE = -E_{HOMO}$ (1)

AE: Electron affinity (eV) $AE = -E_{LUMO}$ (2)

ΔE_g: Energy gap (eV) $\Delta E_g = E_{LUMO} - E_{HOMO}$ (3)

χ: Absolute electronegativity (eV):

$$\chi = \frac{IE+AE}{2} = \frac{-1}{2}(E_{HOMO} + E_{LUMO}) \quad (4)$$

η: Global hardness (eV):

$$\eta = \frac{IE-AE}{2} = -\left(\frac{E_{HOMO}-E_{LUMO}}{2}\right) \quad (5)$$

σ: Global softness $(eV)^{-1}$ $\sigma = -\frac{2}{E_{HOMO}-E_{LUMO}} = 1/\eta$ (6)

ω : Global electrophilicity index (eV):

$$\omega = \frac{\mu^2}{2\eta} = \frac{E_{HOMO}+E_{LUMO}}{8} = \frac{\chi^2}{2\eta} \quad (7)$$

ε : Nucleophilicity $(eV)^{-1}$ $\varepsilon = \frac{1}{\omega}$ (8)

ΔE_{b-d} : Energy of back donation (eV):

$$\Delta E_{b-d} = -\frac{\eta}{4} = \frac{1}{8}(E_{HOMO} - E_{LUMO}) \quad (9)$$

The fraction of electron transferred from the inhibitor molecule to the iron surface was calculated from the obtained values of χ and η as follows [17]:

ΔN : Fraction of electron(s) transfer $\Delta N = \frac{\chi Fe - \chi Inh.}{2(\eta Fe + \eta Inh)}$ (10)

Whereas ηFe and ηinh relate to the absolute hardness of Fe and the inhibitor molecule, respectively, χFe and χinh denote the absolute electronegativity of Fe and the inhibitor molecule. By assuming that for a metallic bulk IP = EA because they are softer information on the local reactivity of the molecule, a theoretical value for the electronegativity of bulk iron was utilized as χFe = 7.0eV and a global hardness of ηFe = 0 in order to determine the fraction of electron transmitted [18].

The Fukui function arises from the observation that an electron will tend to distribute if it is added to an N-electron molecule in order to reduce the energy of the ensuing (N + σ)-electron system. The nucleophilic (f^+) and electrophilic (f^-) Fukui functions, which may be calculated using the finite difference approximation as follows given the corresponding changes in electron density [17-21]:

$f^+ = (\delta p(r)/(\delta N)v^+ = q(N+1) - q(N)$ (11)

$f^- = (\delta p(r)/(\delta N)v^- = q(N) - q(N-1)$ (12)

Where, respectively, q(N+1), q(N), and q(N-1) denote the atom's Mulliken and Hirshfield charges as well as its electron density. Equation (13) was utilized to further define the electrophilic or nucleophilic nature of the whole molecule (global reactivity) using the second order Fukui function:

Second order function: $f(r) = f^+ - f^- = f^2$ (13)

2.2 Molecular dynamic simulation

The Forcite quench molecular dynamic simulation included in the BIOVIA Material Studio software 8.0 Inc. was used to investigate the interaction between the inhibitor molecule and the Fe surface. Each unique inhibitor molecule was sampled by five different lower energy minima of the quenched dynamics in order to determine an average energy minimum [22]. Out of the many Fe surfaces that were accessible, the cleaved Fe(1 1 0) plane was chosen and used because of its stability and more densely packed atoms [2]. Condensed-phase optimized molecular potentials for atomistic simulation studies (COMPASS) force field and the clever method were used to run simulations on a 6 x 5 supercell of the Fe(1 1 0) surface. The constructed Fe slab was significantly relative larger than the molecule to fully accommodate the adsorbed molecule in order to prevent potential molecular edging effects that may occur during the docking process. The completely optimized molecule and Fe(1 1 0) surface were utilized for the docking procedure, along with the NVE ensemble, 5ps simulation period, and 1 fs time step. The simulation temperature was adjusted to 350K. Every 250 steps, the system was quenched on to the optimized Fe(1 1 0) surface atoms being tightly bound. Equations (14) and (15) were utilized to determine the adsorption (E_{ads}) and binding (E_{bind}) energies of the single molecule adsorption on the Fe(1 1 0) surface, allowing access to linking them to inhibitory efficiencies [8,23]:

$$E_{ads} = E_{complex} - (E_{inhibitor} + E_{Fe\ surface}) \quad (14)$$

$$E_{bind} = -E_{ads} \quad (15)$$

Where $E_{Fe\ surface}$ is the energy of the Fe(1 1 0) surface without the inhibitor, $E_{inhibitor}$ is the energy of the inhibitor alone, and $E_{complex}$ is the sum of the energies of the Fe(1 1 0) surface and the inhibitor.

3. Results and Discussion

3.1 Quantum chemical calculations

3.1.1 Equilibrium geometry structure

After completing a comprehensive optimization of their geometry, the bond length (Å) and bond angle (°) of the studied molecules; 2-TCA, 2-TCAH and THIO were computed at the B3YLP functional and DNP basis set in aqueous phase. The results are shown in Table 1. The C-S single bond (1.717 nm) in the thiophene molecule of both molecules has a greater bond length than the C-C double bond (1.413 nm) and C-C single bond (1.368 nm) of both molecules, as can be seen in Table 1. Because all the atoms in the molecules that make up the bond length are the same and are placed on the atoms, they all have equivalent bond length values, which is not surprising. The conjugation between the carbon atom and the sulfur atom, which results in increased bond length in all the molecules, may be responsible for the molecules' average bond length.

From Table 1, it is clear that all of the bond angles in the thiophene rings of all the molecules fall within the same and comparable range of 111.256 to 115.886°. These angles are nearer to 120°, suggesting that the atoms in the investigated molecule's thiophene rings are in the sp^2 hybridized state. In 2-TCA, the bond angles for the carboxylic acid functional group range from 30.208 to 91.872°, but in 2-TCAH, the bond angles range from 31.718 to 149.258°. According to the results, the examined molecule's optimized geometry exhibited a perfect planar geometrical arrangement on the heterocycle but a general trigonal orientation as a result of side chains other than those found in the reference molecule THIO.

3.1.2 Frontier orbitals, energies and derived parameters

Quantum chemical computations are increasingly used in corrosion investigations due to their accuracy and lack of human error [24]. This study investigated the selectivity of the inhibitors and proposed a potential interaction between the inhibitor molecules and the metal surface [25]. The electronic properties of the inhibitor, such as the presence of pi-bonds (partial charges on the molecules), electron density, etc., are what control the inhibition reactivity [26]. These properties are regulated by the type of functional groups that are present in the inhibitor's molecule. The kind of the LUMO, HOMO, and total electron density overlap also affects how the molecules interact with the metal surface because local and global reactivity of the interaction are computed from the resulting HOMO and LUMO eigen values data. The LUMO orbital designates the site of the molecule's electrophilic attack, while the HOMO region designates the locations of nucleophilic assault [26-27]. The molecule can either donate electron(s) to the iron's empty d-orbital (nucleophilic) or accept electron(s) from the metal surface to an electrophilic region of itself depending on how the molecules interact with the metal surface [30–31]. In Figure 2, the white H, gray **C**, blue **N**, yellow **S** and red **O** and other hues show how the atoms in the molecules may be distinguished.

The discovery of the electron has greatly aided in understanding the behaviour of molecular entities, showing that an atom is not a void space and that a molecule's chemical reactivity depends on the electronic distribution of its molecular orbitals [32]. The three examined compounds' full structures can be seen in Figure 2, which indicates that the entire molecule may come into touch with the metal surface and may be able to participate in the adsorption on the surface [33]. The sulphur heteroatom of the molecules is discovered to be surrounded by the HOMO orbitals of THIO, 2-TCA, and 2-TCAH. We discovered that each molecule had a unique LUMO orbital position. This suggests that the compounds may be effective inhibitors due to their electron-donating activity, which is represented by the fact that all of their HOMO orbitals are located around the examined molecules' electron-rich heteroatoms [34].

The interaction between the reacting inhibitor molecules' lowest unoccupied molecular orbital (LUMO) and highest occupied molecular orbital (HOMO) determines a molecule's chemical reactivity. The energy of the E_{HOMO} molecule characterizes the molecule's sensitivity to attack by electrophiles and is directly connected to the ionization potential. Higher E_{HOMO} values are probably indicative of the molecule's propensity to donate electrons to suitable acceptor molecules with low energy or vacant d-orbitals. The energy of LUMO characterizes the molecule's susceptibility to attack by nucleophiles and is

closely correlated with the electron affinity. The ability of the molecules to take electrons is inversely correlated with E_{LUMO} values. Table 2 shows that when the values of E_{HOMO} and E_{LUMO} of the two molecules under study were compared to those of the reference molecule THIO, the values of the inhibitors' E_{HOMO} and E_{LUMO} rise and fall, respectively. This shows that after being adsorbed on the Fe surface, the inhibitors' abilities to donate and accept electrons have increased. Even though THIO was not included, this trend in E_{HOMO} values follows the pattern; THIO > 2-TCAH > 2-TCA, which is in good agreement with the experimentally published results [13]. Dipole moment is a metric used to describe how inhibitor compounds interact in a charged environment. According to several researchers, it is frequently challenging to associate an inhibitor molecule's dipole moment with inhibition effectiveness [2, 35]. Table 2 showed that the dipole moment value followed the following order: 2-TCAH > 2-TCA > THIO, which is inconsistent with the order from which the experimental results were derived. Based on Equations (3) (5), and (6), differences between the global hardness and softness and the energy of the LUMO-HOMO values were all estimated. The chemical hardness and softness (HSAB) theory can be used to define these properties and the activity of molecules is also shown by these properties. According to Table 2, the reference molecule THIO and 2-TCA have a small energy gap. The likelihood that the molecule has strong inhibitory efficiency increases with decreasing energy gap and hardness values [36].

Another factor related to the electrical configuration of the molecule is ionization potential (IP) and electron affinity (EA). The IP and EA values increase as the HOMO and LUMO values decrease [29]. This establishes the electron movement in a field's high polarizability and good donor characteristics. The reference molecule THIO has the lowest IP and EA values compared to other molecules, as can be shown in Table 2. Each inhibitor molecule transmitted fewer than 3.6 electrons to the surface of the iron metal, indicating that this is the primary mechanism by which the molecules' ability to inhibit is accomplished [37, 38]. The molecule with the highest ΔN content has the potential to be the most effective at inhibiting corrosion. The reference molecule THIO has relatively the greatest value of ΔN in the current studies.

The energy of the back donation ΔE_{b-d} can also be used to describe how the inhibitor molecule interacts with the metal surface. According to Umaru and Ayuba [35], the procedure of back donation is encouraged if the energy of back donation (ΔE_{b-d}) value is negative and global hardness is positive. While the global hardness values for both molecules in Table 2 are negative, the global hardness values for the iron metal are positive, indicating that the transfer of charge from the inhibitor molecules to the iron metal occurs during the interaction of the inhibitor molecules with the iron surface. The inverse of electrophilicity (1/ω), nucleophilicity (ε) denotes the propensity of molecules to donate or share electrons, whereas the electrophilicity index (ω) denotes the capacity of molecules to accept electrons [39]. According to research, compounds with high nucleophilicity values are effective corrosion inhibitors whereas molecules with high electrophilicity index values are not [40]. It is clear that the reference molecule THIO has the lowest electrophilicity index and the highest nucleophilicity, making it a superior corrosion inhibitor on the iron surface than the other molecules studied.

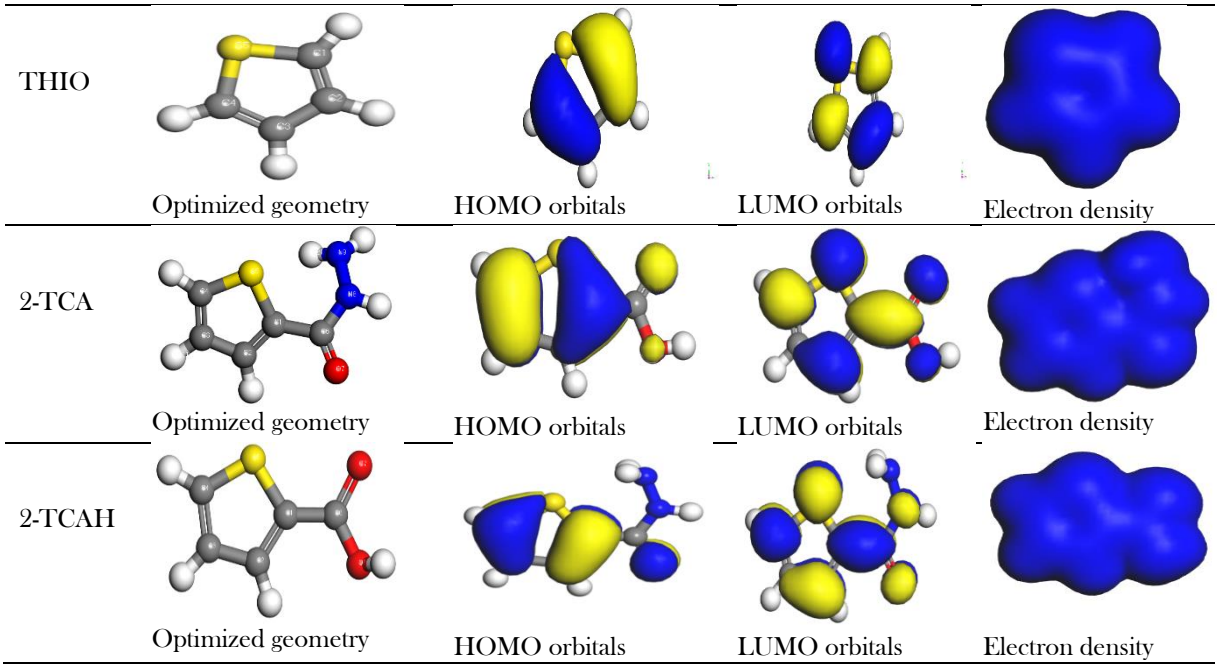

Figure 2. Optimized geometry, HOMO orbitals, LUMO orbitals and electron density of the studied compounds at B3YLP functional and DNP basis set in aqueous phase.

Table 1: Geometric parameters of the optimized studied molecules

Bond length (Å)	THIO	2-TCA	2-TCAH	Bond angle (°)	THIO	2-TCA	2-TCAH
C_1-C_2	1.368	1.375	1.376	C_1-C_2-C_3	112.654	113.115	113.391
C_2-C_3	1.413	1.411	1.402	C_2-C_3-C_4	112.654	112.131	112.385
C_3-C_4	1.368	1.370	1.371	C_3-C_4-S_5	111.256	112.668	111.912
C_4-S_5	1.712	1.717	1.705	C_4-S_5-C_6	-	118.067	115.886
S_5-C_6	-	2.768	2.862	S_5-C_6-O_7	-	91.872	149.258
C_6-O_7	-	1.220	1.239	C_6-O_7-O_8	-	30.208	-
O_7-O_8	-	2.252	-	C_6-O_7-N_8	-	-	31.718
O_7-N_8	-	-	2.242	O_7-N_8-N_9	-	-	136.267
N_8-N_9	-	-	1.377				

Table 2: Calculated quantum chemical parameters of the studied compounds

Properties	THIO	2-TCA	2-TCAH
E_{HOMO} (eV)	-5.564	-7.111	-6.471
E_{LUMO} (eV)	-0.519	-1.978	-1.176
ΔE (eV)	5.045	5.133	5.295
μ (debye)	1.201	1.740	2.014
IP (eV)	5.564	7.111	6.471
EA (eV)	0.519	1.978	1.176
η	2.523	2.567	2.648
σ	0.396	0.389	0.378
χ	3.042	4.545	3.824
ω (eV)	1.834	4.024	2.761
ε (eV)	0.545	0.249	0.362
ΔE_{b-d} (eV)	-0.630	-0.641	-0.662
ΔN	0.784	0.478	0.599

3.1.3 Active centres

It's important to keep in mind that inhibitor molecules can bond with metal surfaces by electron transfer (giving or taking an electron from the reactive species), which can help identify the active site on the inhibitor molecule. The active sites of interaction between the inhibitor compounds under nucleophilic (f⁻) and electrophilic (f) attack were investigated using the Fukui indices. The maximal threshold values of f⁻ and f regulate the nucleophilic and electrophilic assaults. The atoms with the highest value of f⁻ are the chosen targets for nucleophilic assaults. Similar to this, electrophilic assaults are preferred in situations when f has the highest value. Table 3 lists the examined inhibitor compounds' computed condensed Fukui functions. As can be observed from the Table, 2-thiophene carboxylic acid (2-TCA) has higher Mulliken and Hirshfeld charges on C(4), S(5), and O(7) atoms, while C(1), C(4) and S(5) are those of THIO which are the regions responsible for nucleophilic attacks and electrophilic attacks on the molecules. It is on the C(4), C(5), and O(7) atoms in 2-thiophene carboxylic acid hydrazide (2-TCAH), respectively. The compounds' labeled atoms are shown in Figure 3. S(5) and C(4) are the most likely points of attack in terms of nucleophilic (f⁻) and electrophilic (f) point of assaults in THIO and 2-TCA molecules when the highest values of both f⁻ and f from Table 3 are taken into account. While C(5) is reported to have the highest values both f⁻ and f for 2-TCAH.

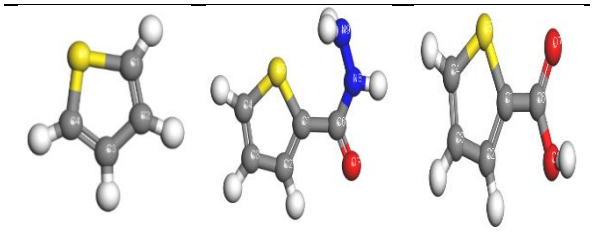

THIO 2-TCA 2-TCAH

Figure 3. Labelled atoms of the studied molecules

Table 3: Calculated Fukui Functions of the studied Inhibitor Molecules

Inhibitors	Atom	Nucleophilic attack (f_k^+)		Electrophilic attack (f_k^-)	
		Mulliken	**Hirshfeld**	**Mulliken**	**Hirshfeld**
THIO	C(1)	0.132	0.142	0.121	0.178
	C(2)	0.041	0.100	0.058	0.107
	C(3)	0.064	0.096	0.030	0.108
	C(4)	0.091	0.138	0.161	0.181
	S(5)	0.252	0.260	0.178	0.180
	H(6)	0.106	0.072	0.119	0.067
	H(7)	0.105	0.062	0.107	0.054
	H(8)	0.095	0.049	0.118	0.067
	H(9)	0.113	0.081	0.109	0.059
2-TCA	C(1)	0.036	0.070	0.141	0.144
	C(2)	0.132	0.112	0.053	0.069
	C(3)	0.025	0.060	0.119	0.132
	C(4)	0.120	0.116	0.148	0.163

	S(5)	0.200	0.186	0.169	0.163
	C(6)	0.123	0.111	0.037	0.043
	O(7)	0.124	0.124	0.083	0.084
	O(8)	0.054	0.063	0.027	0.032
	H(9)	0.059	0.048	0.056	0.037
	H(10)	0.046	0.031	0.071	0.054
	H(11)	0.055	0.050	0.074	0.060
	H(12)	0.028	0.030	0.021	0.020
2-TCAH	C(1)	0.054	0.076	0.114	0.129
	C(2)	0.084	0.097	0.054	0.084
	C(3)	0.016	0.067	0.043	0.079
	C(4)	0.101	0.117	0.112	0.145
	C(5)	0.188	0.179	0.152	0.137
	C(6)	0.063	0.069	0.013	0.031
	O(7)	0.103	0.096	0.125	0.119
	N(8)	0.032	0.045	0.020	0.031
	N(9)	0.032	0.033	0.030	0.033
	H(10)	0.073	0.048	0.081	0.042
	H(11)	0.083	0.044	0.087	0.048
	H(12)	0.086	0.059	0.094	0.061
	H(13)	0.051	0.036	0.043	0.029
	H(14)	0.018	0.019	0.016	0.013
	H(15)	0.019	0.013	0.016	0.019

The examined inhibitor compounds' computed percentage of second-order Fukui function is shown in Table 4; the graphical representations are shown in Figure 4. According to Table 4, 44.44% of the elements in Figure 4 had positive values of the Fukui second order function ($f^2 > 0$), whereas 55.55% had negative values ($f^2 < 0$) in the THIO molecule. Similar to the 2-TCA molecule, 41.67% of the element displayed negative values on Figure 4 of the second order Fukui function, whereas 58.33% of the element displayed positive values. On the other hand, in 2-TCAH, 46.67% of the elements displayed negative values for the second order Fukui function, while 53.33% of the elements showed positive values. It can be deduced from the second order Fukui functions of the reference molecule and the two investigated inhibitor molecules that THIO is more electrophilic than 2-TCA and 2-TCAH and, as a result, more efficient at preventing the corrosion of iron metal surfaces [40].

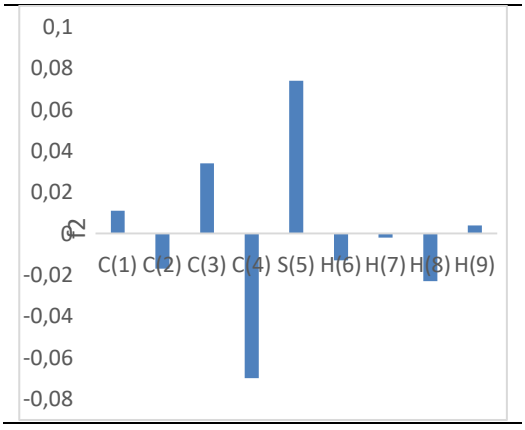

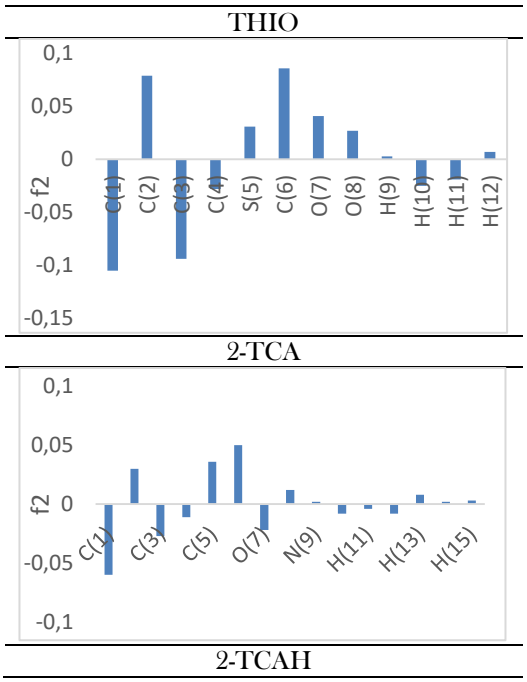

Figure 4. Second-order Fukui function of the studied compounds

Table 4: Calculated percentage of second- order Fukui function of the studied inhibitor molecules

Inhibitors	Nucleophilic (F^{2+})	Electrophilic (F^{2-})
THIO	44.44	55.55
2-TCA	58.33	41.67
2-TCAH	53.33	46.69

3.2 Molecular Dynamic Simulation

A molecular level analysis of the interactions between each inhibitor molecule and the Fe(1 1 0) surface was accomplished by utilizing Forcite quench to sample a wide range of low-energy configurations and locate the low-energy minima [24, 39]. Figure 5 depicts a snapshot of the top-view equilibrium configurations of the simulated systems. Table 5 lists the pertinent computed energy parameters of the simulated systems. As seen in Figure 5, the inhibitor molecules' heteroatoms and the portion of the molecule containing the aromatic rings are adsorbed on the surface of Fe(1 1 0) in a nearly flat orientation, ensuring the inhibitor molecules' best contacts with the metallic surface.

The computed binding/adsorption energies for each inhibitor molecule on the Fe(1 1 0) metal surface are shown in Table 5. These results were obtained by averaging the energy of the representative adsorption configurations that were the most stable. Table 5 shows that the computed adsorption energy value for the reference molecule THIO is -30.45 kcal/mol, while it is -23.758 kcal/mol for 2-TCA and -

6.442 kcal/mol for 2-TCAH. These threshold values, which were all negative and small in magnitude, indicate stable adsorption structures [15]. The reference molecule THIO has a higher potential for inhibition efficacy than molecules 2-TCA and 2-TCAH, according to the computed adsorption energy of the investigated inhibitor molecule, which follows the trend; THIO > 2-TCA > 2-TCAH. Even though the simulations did not account for the specific covalent interactions between the molecules and the iron surface, the magnitudes of the predicted binding energies were all less than 100 kcal/mol (Table 5). According to reports, this value falls within the range of physisorption interactions [32, 39, 41]. Additionally, it has been noted that the better the inhibitor adsorption onto the metal surface and, thus, the higher the inhibition efficacy, the more negative the adsorption energy of the inhibitor-metal surface is or the more positive the binding energy value [42–45].

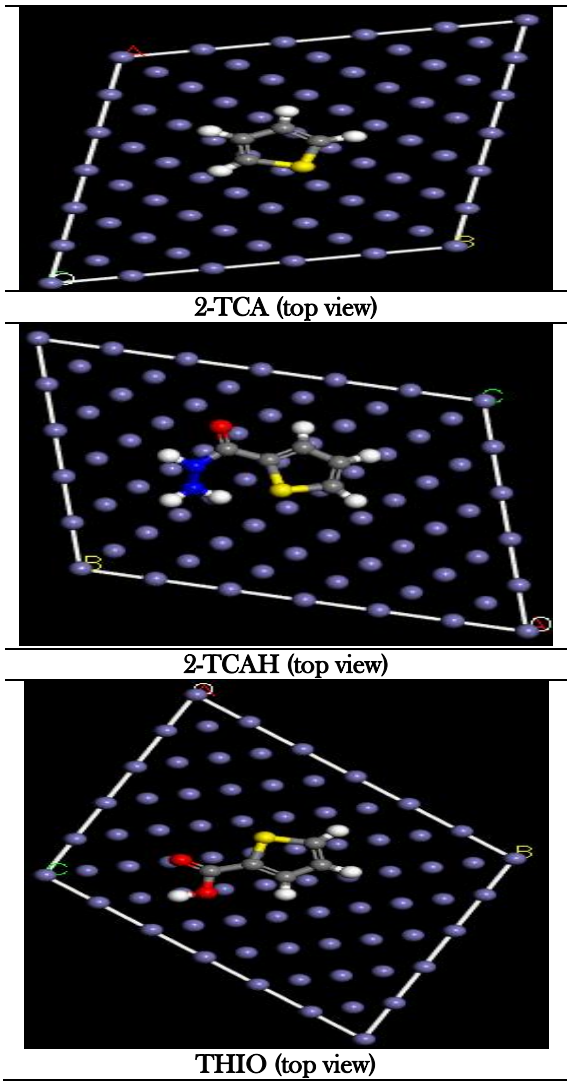

Figure 5. Configuration of THIO, 2-TCA, 2-TCAH molecules adsorbed on Fe(110) surface

Table 5: Energy parameters (kcal/mol) associated with the adsorption of the inhibitor molecules on Fe (110) surface in aqueous phase.

Property	THIO	2-TCA	2-TCAH
Total Energy (kcal/mol)	11.78± 0.0014	-79.21± 0.458	-10.95±0.394
Energy of Molecule (kcal/mol)	- 18.66± 0.0019	- 55.449 ±0.918	-4.508±0.798
Energy of Fe(1 1 0) Surface (kcal/mol)	0.00± 0.00	0.00± 0.00	0.00±0.00
Adsorption Energy (kcal/mol)	- 30.45± 0.0018	- 23.758 ±0.789	-6.442±0.300
Binding Energy (kcal/mol)	30.45± 0.0018	23.758 ±0.789	6.442±0.300

To determine how each molecule interacted with the metal surface, bond length and bond angles were also measured before and after the inhibitor molecule adhered to the Fe(1 1 0) surface. Table 6a–c displays the findings from the assessment of bond length and bond angles of each inhibitor molecule on the Fe(1 1 0) metal acquired from molecular structures corresponding to each molecule's lowest energy state before and after the quenched simulation. Table 6a shows that, with the exception of C1-C2 and C2-C3 bonds, the bond length of THIO changed at the C3-C4 and C4-S5 atoms during THIO's adsorption on Fe(1 1 0). All of the estimated bond angles for the THIO molecule on Fe (1 1 0), as seen in Table 6a, were changed, possibly as a result of molecular contact with the Fe(1 1 0) surface. In Table 6b, for 2-TCA, four bond lengths; S5-C6, C6-O7, O7-N8, and N8-N9 were all altered as a result of molecular contact with the metal's surface. Similar to this, the whole bond angles of 2-TCA alter, possibly as a function of the molecule's contact with and inhibition by the surface. Table 6c shows the bond lengths of 2-TCAH before and after adsorption on the metal and reveals modifications in four of the bonds, including; C1-C2, C2-C3, C4-S5, and S5-C6. The molecular contact caused the molecule to alter. On the other hand, 2-TCAH's bond angles all changed, which might be a result of inhibition or the molecule's interaction with the surface of the iron. In a nutshell, it can be said that the variation in the inhibitor molecules' bond lengths and angles before and after they have been adsorbed on the metal surface demonstrates the inhibitors' involvement in the inhibition process. The closeness in the functional groups of the examined compounds may account for the similarities in bond length and bond angles.

Table 6a: Bond length (A^0) and bond angle (^{0}) parameters of the optimized THIO molecule before and after adsorption on Fe(1 1 0) surface

Bond length	Before adsorption	After adsorption
C_1-C_2	1.371	1.371
C_2-C_3	1.415	1.415
C_3-C_4	1.371	1.372
C_4-S_5	1.724	1.725
Bond angle	**Before adsorption**	**After adsorption**
C_1-C_2-C_3	112.887	112.929
C_2-C_3-C_4	112.868	112.876
C_3-C_4-S_5	111.118	112.062

Table 6b: Bond length (A^0) and bond angle (^{0}) parameters of the optimized 2-TCA molecule before and after adsorption on Fe(1 1 0) surface

Bond length	Before adsorption	After adsorption
C_1-C_2	1.368	1.368
C_2-C_3	1.411	1.411
C_3-C_4	1.375	1.375
C_4-S_5	1.720	1.720
S_5-C_6	2.255	2.251
C_6-0_7	1.216	1.217
O_7-N_8	2.255	2.251
N-N_9	1.441	1.440
Bond angle	**Before adsorption**	**After adsorption**
C_1-C_2-C_3	112.996	113.386
C_2-C_3-C_4	113.151	113.049
C_3-C_4-S_5	110.773	110.701
C_4-S_5-C_6	118.706	118.198
S_5-C_6-O_7	149.298	151.703
C_6-O_7-N_8	31.697	32.136
O_7-N_8-N_9	141.241	155.995

Table 6c: Bond length (A^0) and bond angle (^{0}) parameters of the optimized 2-TCAH molecule before and after adsorption on Fe(1 1 0) surface

Bond length	Before adsorption	After adsorption
C_1-C_2	1.368	1.369
C_2-C_3	1.411	1.410
C_3-C_4	1.375	1.375
C_4-S_5	1.720	1.721
S_5-C_6	2.785	2.788
C_6-O_7	1.215	1.215
O_7-O_8	2.219	2.219
Bond angle	**Before adsorption**	**After adsorption**
C_1-C_2-C_3	112.819	112.865
C_2-C_3-C_4	113.188	113.222
C_3-C_4-S_5	110.758	110.737
C_4-S_5-C_6	119.301	118.947
S_5-C_6-O_7	96.420	96.564
C_6-O_7-O_8	32.407	32.445

4. Conclusions

From the current investigation, the following findings may be drawn:

• The aggregated quantum chemical parameters determined for the inhibitor molecule electronic structures revealed that their inhibitory capacity follows the following hierarchy: THIO > 2-TCA > 2-TCAH.

• Local reactivities determined by Fukui indices revealed that the inhibitor molecules' site of connection with the iron surface most likely stems from their heteroatoms of sulfur, oxygen, or nitrogen, which are abundant in n-electrons.

• With a postulated mechanism of physical adsorption, the predicted adsorption/binding energy values obtained were negative and low, indicating relatively poor adsorption and inhibition.

• Analysis of bond lengths and angles for the geometrically optimized investigated molecules before and after adsorption revealed that the molecules do not lie flat on the surface of the Fe(1 1 0) surface in a perfect orientation.

• In conclusion, it was discovered that the reference molecule THIO was a more effective inhibitor on iron surface than 2-TCA and 2-TCAH. This finding may be related to THIO's substantially more planar structure, which will improve its better adsorption on the surface of the Fe(1 1 0) surface.

Acknowledgments

The authors wish to thank Dr, David Ebuka Arthur of the Department of Pre and Applied Chemistry, University of Maiduguri, Borno for the initial installation of BIOVIA Materials Studio Inc. Software.

References

[1] M. A. Hegazy, S. S. Abd El Rehim, A. M. Badawia, M. Y. Ahmed, RSC Adv., *5* (2015) 49070–49079. doi: 10.1039/c5ra05388a.

[2] T. A. Nyijime, I. Iorhuna, Appl. J. Envir. Eng. Sci. 8(2) (2022) 177-186.

[3] A. Popova, M. Christov, S. Raicheva, E. Sokolova, Corros. Sci. 46 (2004)1333–1350.
[4] M. Sahin, G. Gece, F. Karci, S. Bilgic, J. Appl. Electrochem. 38 (2008) 809–815.
[5] X. He, J. Mao, Q. Ma, Y. Tang, Mol. Liq. (2018). doi: 10.1016/j.molliq.2018.08.021.
[6] W. Li, Z. Zhang, Y. Zhai, L. Ruan, W. Zhang, L. Wu, Int. J. Electrochem. Sci. 15 (2020) 722 – 739. doi: 10.20964/2020.01.63.
[7] S. A. Umoren, E. E. Ebenso, Pigment and Resin Technology, 37 (2008) 173–182. http://dx.doi.org/10.1108/03699420810871020.
[8] T. A. Nyijime, A. M. Ayuba, Appl. J. Envir. Eng. Sci. 6(4) (2020) 344-355.
[9] A. M. Ayuba, U. Umaru, Karbala International Journal of Modern Science, 7(3) (2021). https://doi.org/10.33640/2405-609X.3119
[10] N. O. Obi-Egbedi, I. B. Obot, M. I. El-Khaiary, S. A. Umoren, E. E. Ebenso, Int. J. Electrochem. Sci., 6 (2011) 5649-5675.
[11] X. Luo, C. Ci, J. Li, K. Lin, S. Du, H. Zhang, X. Li, Y. F. Cheng, J. Zang, Y. Liu, Corros. Sci., 151 (2019) 132e142. https://doi.org/10.1016/j.corsci.2019.02.027.
[12] I. B. Obot, N. O. Obi-Egbedi, E. E. Ebenso, A. S. Afolabi, E. E. Oguzie, Res. Chem. Intermed., 39 (2013) 1927e1948. https://doi.org/10.1007/s11164-012-0726-3.
[13] A. S. Fouda, A. A. Ibrahim, W. T. El-behairy, Der Pharma Chemica, 6(5) (2014) 144-157.
[14] Materials Studio 6.1 Manual, Accelrys, Inc., San Diego, CA, (2007).
[15] A. M. Ayuba, T. A. Nyijime, Journal of applied science and environmental studies, 4(2) (2021) 393-405.
[16] T. Koopmans, Physica., 1 (1993) 104-113.
[17] K. F. Khaled, Electrochim. Acta, 22 (2010) 6523.
[18] R. G. Pearson, J. Am. Chem. Soc, 85(22) (1963) 3533-3539.
[19] R. G. Parr, L. Szentpaly, S. Liu, J. Am. Chem. Soc, 121 (1999) 1922-1924.
[20] G. Bereket, E. Hur, C. Ogretir, J. Mol. Struct. (Theochem). 578 (2002) 79e88. https://doi.org/10.1016/S0166-1280(01)00684-4.
[21] M. Belghiti, S. Echihi, A. Dafali, Y. Karzazi, M. Bakasse, H. Elalaoui-Elabdallaoui, Applied surface science. 491 (2019) 707-22.
[22] G. Bereket, C. Ogretir, A. Yurt, J. Mol. Struct. (Theochem) 571 (2001) 139e145, https://doi.org/10.1016/s0166- 1280(01)00552-8.
[23] B. Gómez, N. V. Likhanova, M. A. Domínguez-Aguilar, R. Martínez-Palou, A. Vela, J. L. Gázquez, J. Phys. Chem. B. 110(18) (2006) 8928-34.
[24] T. V. Kumar, J. Makangara, C. Laxmikanth, N. S. Babu, International journal of computational and theoretical chemistry 4 (2016) 1-6.
[25] S. J. Smith, B. T. Sutcliffe, Review in computational chemistry 10 (1972) 271-316.
[26] I. B. Obot, Z. M. Gasem, S. A. Umoren Int. J. Electrochem. Sci. 9 (2014) 2367-2378.
[27] K. F. Khaled, M. A. Amin, Electrochimica Acta 53(9) (2008) 3484-3492.
[28] W. Li, Z. Zhang, Y. Zhai, L. Ruan, W. Zhang, L. Wu, International Journal of Electrochemical Science (15) (2020) 722–739.
[29] H. Lgaz, S. Masroor, M. Chafiq, M. Damej, A. Brahmia, R. Salghi, Construction and Building Materials 10(3) (2020) 357.
[30] W. Kohn, A. D. Becke, R. G. Parr, The journal of physical chemistry 100(31) (1996) 12974-12980.
[31] K. F. Khaled, N. S. Abdel-Shafi, N. A. Al-Mobarak, Int. J. Electrochem. Sci. (7) (2012)1027 – 1044.
[32] A. M. Ayuba, A. Uzairu, H. Abba, G. A. Shallangwa, Moroccan journal of chemistry 6(1) (2018) 160-172.
[33] A. M. Ayuba, A. Aminullahi, Algerian Journal of Engineering and Technology (03) (2021) 028–037.
[34] F. Benhiba, R. Hsissou, K. Abderrahim, H. Serrar, Z. Rouifi, S. Boukhris, A. Zarrouk, Journal of Bio- and Tribo-Corrosion 8(2) (2022) 1-15.
[35] U. Umaru, A. M. Ayuba, RHAZES: Green Appl. Chem. 10 (2020) 113e128, https://doi.org/10.48419/IMIST.PRSM/rhazes-v10.23814
[36] L. Guo, M. Zhu, J. Chang, R. Thomas, R. Zhang, P. Wang, International Journal of Electrochemical Science. 16(2) (2021) 211139.
[37] H. Zhang, Y. Chen, Z. Zhang, Result Phys. 11 (2018) 554-63.
[38] M. Talari, S. M. Nezhad, S. J. Alavi, M. Mohtashamipour, A. Davoodi, S. Hosseinpour, J. Mol. Liq. 286 (2019)110915.
[39] J. Frau, D. Glossman-Mitnik, Front. Chem. 5 (2017) 16.
[40] L. Guo, Z. S. Safi, S. Kaya, W. Shi, B. Tüzün, N. Altunay, Front. Chem. 6 (2018) 155.
[41] T. F. Maryer, C. Gehlen, C. Deuberschmidt, 16-Corrosion monitoring in concrete, Woodhead publishing series in metals and surface engineering 2021; p 379-405. doi.org/10.10161b978-0-08-103003-5-00016-3.
[42] S. John, J. Joy, M. Prajila, A. J. Joseph, Materials and corrosion 62(11) (2011) 1031-41.
[43] A. M. Ayuba, A. Ameenullah, Algerian Journal of Engineering and Technology 3 (2020) 028-37.
[44] K. M. Zohdy, R. M. El-Sherif, S. Ramkumar, A. M. El-Shamy, Upstream Oil Gas Technol 6 (2021) 100025.
[45] E. Alibakhshi, M. Ramezanzadeh, G. Bahlakeh, B. Ramezanzadeh, M. Mahdavian, M. Motamedi, J. Mol. Liq. 255 (2018)185–198.